

1 **Method to calculate the aerosol asymmetry factor based on measurements from**
2 **the humidified nephelometer system**

3 **Gang Zhao¹, Chunsheng Zhao¹, Ye Kuang², Yuxuan Bian³, Jiangchuan Tao², Chuanyang Shen¹,**
4 **Yingli Yu¹**

5 ¹Department of Atmospheric and Oceanic Sciences, School of Physics, Peking University, Beijing,
6 China

7 ²Institute for Environmental and Climate Research, Jinan University, Guangzhou 511443, China

8 ³State Key Laboratory of Severe Weather, Chinese Academy of Meteorological Sciences, Beijing,
9 100081, China

10 Corresponding author: Chunsheng Zhao (zcs@pku.edu.cn)

11 **Abstract**

12 The aerosol asymmetry factor (g) is one of the most important factors for assessing direct aerosol
13 radiative forcing. So far, few studies have focused on the measurements and parameterization of g . The
14 characteristics of g are studied based on field measurements over the North China Plain by using the
15 Mie scattering theory. The results show that calculated g values for the dry aerosol can vary over a
16 wide range (between 0.54 and 0.67). When ambient relative humidity (RH) reaches 90%, g is
17 significantly enhanced by a factor of 1.2 due to aerosol hygroscopic growth of the continental aerosol.
18 For the first time, a novel method to calculate g based on measurements from the humidified
19 nephelometer system is proposed. This method can constrain the uncertainty of g within 2.56% for dry
20 aerosol populations and 4.02% for ambient aerosols, taking into account aerosol hygroscopic growth.
21 Sensitivity studies show that aerosol hygroscopicity is the most important factor that influences the
22 accuracy of predicting g .

23 **1 Introduction**

24 In addition to aerosol optical depth and aerosol single-scattering albedo, the aerosol phase function
25 is the most important factor for assessing direct aerosol radiative forcing (DARF) (Andrews et al.,
26 2006; Russell et al., 1997). The Henyey-Greenstein (HG) phase function (PF_{HG}) is a widely used
27 method to parameterize the phase function (Toublanc, 1996; Boucher, 1998; Pandey and Chakrabarty,
28 2016) because it uses the aerosol asymmetry factor (g) as the only free parameter. The PF_{HG} is
29 expressed as

hello 2018/4/24 8:57 PM

已删除: Direct aerosol radiative forcing can
be reduced by 40% when g increases by 20%.

hello 2018/4/24 2:12 PM

已删除: ambient RH and

hello 2018/4/24 2:12 PM

已删除: are

hello 2018/4/24 2:12 PM

已删除: s

hello 2018/4/24 12:55 PM

已删除: HG phase function

36
37
38
39
40
41
42
43
44
45
46
47
48
49
50
51
52
53
54
55
56
57
58
59
60
61
62
63
64

$$P_{HG}(\theta) = \frac{1-g^2}{(1+g^2-2g\cos\theta)^{3/2}} \quad (1)$$

where θ is the angle between the incident light direction and the scattered light direction. In this respect, the free parameter g can reflect the angular aerosol scattering energy distribution. g is defined as:

$$g = \frac{1}{2} \int_0^\pi \cos \theta P(\theta) \sin(\theta) d\theta \quad (2)$$

where $P(\theta)$ is the normalized scattering phase function. As a result, g can be a computationally efficient factor that replaces the phase function to study aerosol radiative transfer properties (Toublanc, 1996; Hansen, 1969; Boucher, 1998). Some researchers have widely accepted the use of g as a replacement of the phase function (Hansen, 1969; Wiscombe and Grams, 1976; Sagan and Pollack, 1967; Andrews et al., 2006). However, the g -related PF_{HG} may cause significant bias when estimating photo-dissociation rates (Toublanc, 1996) and aerosol radiative forcing effects (Boucher, 1998). Up to now, there have been few studies that have assessed the bias when replacing the ambient phase function with the g -related PF_{HG} (Pandey and Chakrabarty, 2016; Boucher, 1998; Wiscombe and Grams, 1976) and there is no study that uses field measurements of aerosol optical properties to estimate the bias. Moreover, variations in g can influence the evolution of the atmospheric vertical structure through its effects on the atmospheric radiative distribution. Kudo et al. (2016) also found that the vertical profile of the asymmetry factor plays an important role in altering vertical variations in the solar heating rate. Marshall et al. (1995) reported that a 10% overestimation of g can systematically reduce aerosol climatic forcing by 12% or more. Andrews et al. (2006) found that a 10% reduction in g would result in a 19% overestimation of atmosphere radiative forcing at the top of atmosphere (TOA). An accurate estimation of g can help improve the assessment of the aerosol radiative effect.

There are many methods to derive the aerosol g for the dry and ambient condition. Horvath et al. (2016) measured the phase function of aerosols, calculated the g of aerosols, and found that the g -related PF_{HG} can be used as a good approximation of the measured phase function. Many works used the Mie model (Bohren and Huffman, 2007) to calculate the phase function and proved its reliability (Andrews et al., 2006; Marshall et al., 1995; Shettle and Fenn, 1979; Bian et al., 2017). Comprehensive attempts have been made to relate g with the hemispheric backscatter fraction (b), where b is the ratio of light scattered into the backward hemisphere compared to total light scattered in all directions (Wiscombe and Grams, 1976; Andrews et al., 2006; Horvath et al., 2016), with the definition of

hello 2018/4/7 6:06 PM
已删除: aerosol

hello 2018/4/24 12:56 PM
已删除: HG phase function

hello 2018/4/24 12:57 PM
已删除: HG phase function

hello 2018/4/8 11:15 AM
已删除: by

hello 2018/4/8 11:16 AM
已删除: using

hello 2018/4/8 11:40 AM
已删除: Though many methods can be used to derive g , there is no available method to measure g directly

hello 2018/4/24 12:57 PM
已删除: HG phase function

$$b = \frac{\int_{\frac{\pi}{2}}^{\pi} P(\theta) \cdot \sin\theta \cdot d\theta}{\int_0^{\pi} P(\theta) \cdot \sin\theta \cdot d\theta} \quad (3)$$

hello 2018/4/8 10:06 AM

已设置格式: 居中

The main advantage of the backscatter ratio is that it can be measured with an integrating nephelometer equipped with a backscatter shutter (Charlson et al., 1974).

hello 2018/4/8 10:07 AM

已设置格式: 缩进: 首行缩进: 0 cm

The free parameter g varies significantly for different aerosol types and different seasons. In the previous, the g values are studied mainly by using the Mie scattering theory and the measured aerosol particle numbers size distribution (PNSD). D'Almeida et al. (1991) suggested that g at a wavelength of 500 nm ranges from 0.64 to 0.83 depending on the aerosol type and season. A mean value of 0.67 at an ambient relative humidity (RH) was also recommended (D'Almeida et al., 1991). Hartley and Hobbs (2001) reported a median g value of 0.7 for aerosols along the east coast of the United States. Formenti et al. (2000) measured Saharan dust aerosol and found that the aerosol g values ranged from 0.72-0.73. Biomass burning aerosols in Brazil had a low g value of 0.54 (Ross et al., 1998).

Some works have studied the impacts of aerosol hygroscopic growth on the parameter g (Hartley and Hobbs, 2001; Kuang et al., 2015; Andrews et al., 2006) and found that variations in g with RH can have significant influences on aerosol radiative effects (Kuang et al., 2015; Kuang et al., 2016; Andrews et al., 2006). A parameterization scheme of g , that takes RH and aerosol hygroscopic growth into account, is necessary.

When exposed to the ambient atmosphere, aerosols can grow by taking up water, which causes their corresponding optical properties to considerable change. The κ -Köhler theory (Petters and Kreidenweis, 2007) is widely used to describe the hygroscopic growth of aerosol particles by using a single aerosol hygroscopic growth parameter (κ) and the κ -Köhler equation, which is shown as

$$\frac{RH}{100} = \frac{gf^3 - 1}{gf^3 - (1 - D)} \cdot \exp\left(\frac{4\sigma_s/a \cdot M_{water}}{R \cdot T \cdot D_d \cdot gf \cdot \rho_w}\right) \quad (4)$$

hello 2018/4/8 5:09 PM

已删除: absorbing

where D_d is the dry particle diameter; $gf(RH)$ is the aerosol growth factor, which is defined as the ratio of the aerosol diameter at a given RH and the dry aerosol diameter (D_{RH}/D_d); T is the temperature; $\sigma_{s/a}$ is the surface tension of the solution; M_{water} is the molecular weight of water. R is the universal gas constant and ρ_w is the density of water. The aerosol hygroscopic growth parameter κ can be further used to investigate the influence of aerosol hygroscopic growth on aerosol optical properties (Tao et al., 2014; Kuang et al., 2015; Zhao et al., 2017) and aerosol liquids water contents (Bian et al., 2014).

hello 2018/4/13 12:52 PM

已删除: 3

104 According to the Mie theory, g is associated with aerosol particle number size distribution, the
105 particle complex refractive index, the aerosol mixing state and ambient RH. At the same time, the
106 aerosol morphology has significant influence on g . Datasets from the humidified nephelometer system
107 can partially account for all of these factors. The humidified nephelometer system consists of two
108 nephelometers: one nephelometer measures dry aerosol scattering properties and the other measures
109 aerosol scattering properties under well-controlled RH conditions. This results in the light scattering
110 enhancement factor (f_{RH}), which is defined as $f_{RH}(\lambda, RH) = \sigma_{sca}(\lambda, RH) / \sigma_{sca}(\lambda, dry)$, or the ratio of the aerosol
111 scattering coefficient under given RH conditions to that of dry conditions. Each nephelometer can
112 provide a scattering coefficient (σ_{sca}) and back-scattering coefficient (β_{sca}) at three wavelengths (450,
113 525, 635nm). σ_{sca} can be used to calculate the aerosol scattering Ångström index, which reflects the
114 aerosol PNSD to some extent. In general, a larger value for the Ångström index always corresponds to
115 a smaller predominant aerosol size. Variations in β_{sca} and σ_{sca} can be used to deduce the aerosol BC
116 mixing state (Ma et al., 2012). At the same time, datasets from the humidified nephelometer system
117 can also be used alone to measure the aerosol hygroscopicity and provide an overall hygroscopic
118 parameter κ (Kuang et al., 2017). All in all, measurements from the humidified nephelometer system
119 might be used for estimating g under the given RH conditions. However, there is no clear relationship
120 between the measured datasets from the humidified nephelometer and g . The non-linear influence of
121 the above listed factors on g makes it difficult to parameterize the g .

122 Random forest machine learning model is a powerful technique that can be used for classification
123 and non-linear regression (Huttunen et al., 2016; Breiman, 2001; Hu et al., 2017). This model is a
124 widely used nonparametric machine learning algorithm that has several strengths. First, it involves
125 fewer assumptions regarding the dependence between observations and outcomes when compared with
126 traditional parametric regression models. Second, strict relationships among variables are not needed
127 before implementing the random forest model. Third, this learning model requires much less
128 computing resource than that of the deep learning. Finally, this model has very low risk of overfitting
129 by averaging over an ensemble of decision trees. Thus, the random forest machine learning model is
130 used in this work to study the calculation of g based on the datasets of the humidified nephelometer
131 system.

132 In this study, the Mie scattering theory and field measurements over the North China Plain (NCP)
133 are used to study the characteristics of g . Section 2 describes the related datasets used in this study.

hello 2018/4/8 5:27 PM

已设置格式: 下标

hello 2018/4/8 5:27 PM

已设置格式: 下标

hello 2018/4/8 10:53 AM

已删除: particle numbers size distribution
(PNSD)

hello 2018/4/16 1:47 PM

已设置格式: 字体:(中文) +中文主题正文

136 Details of the study on the characteristics of g and impacts of aerosol hygroscopic growth on g are
137 shown in section 3.1. A new method, which is based on a random forest machine learning model, is
138 introduced to calculate g in section 3.2. We also discuss the impacts of g variations on the uncertainties
139 of DARF in section 3.3, and the corresponding results are presented in section 4.3. Section 4.1 gives
140 the calculated characteristics of g and section 4.2 proves the feasibility of using the machine learning
141 model to calculate g . At the same time this method is validated by the ambient aerosol phase function
142 measured with a charge-coupled device -laser aerosol detective system (CCD-LADS). Conclusions are
143 in section 5.

144 2. Instruments and datasets

145 Datasets used in this study come from three field campaigns, which were conducted at three
146 different sites in the NCP. The three field measurements are conducted at Gucheng in Hebei Province
147 (Gucheng, 39°09' N, 115°44' E) from 15 October to 25 November in 2016, the AERONET
148 BEIJING_PKU station in Beijing (PKU, 39°59' N, 116°18' E) from 21 March to 10 April in 2017, and
149 the Yanqi Campus of the University of Chinese Academy of Sciences (UCAS, 40°24' N, 116°40' E) in
150 the Huairou district, Beijing from 3 January to 27 January in 2016. Details of these locations are
151 shown in Fig. S1. The PKU station is located at the northwest of Beijing, between the 4th and 5th ring
152 road. Datasets for this location are representative of urban aerosols in the NCP. Gucheng is located
153 between two megacities (120 km from Beijing and 190 km from Shijiazhuang) of NCP and the
154 pollution conditions of Gucheng can be a good representation of the continental background in the
155 NCP. Details for the Gucheng station can be found at Kuang et al. (2017). The UCAS station is 60 km
156 away from the center of Beijing and is at the edge of the NCP, which makes it suitable for measuring
157 the regional pollution properties of the NCP (Ma et al., 2016). More details of the measurement sites
158 can refer to section 1 of the supplementary materials.

159 Table 1 lists the information for the field campaigns and the datasets used in this study. During the
160 campaigns, sampled aerosols that had an aerodynamic diameter of less than 10 μm are selected by an
161 impactor (Mesa Labs, Model SSI2.5) at the inlet. These aerosols are then dried to below 30% RH with
162 a Nafion drying tube and then lead to each instrument. Aerosol PNSDs ranging from 3 nm to 10 μm
163 are measured by using the scanning mobility particle size spectrometer (SMPS, TSI Inc., model 3936)
164 and an aerodynamic particle sizer (APS, TSI Inc., model 3321) with a temporal resolution of 5 min.
165 Black carbon (BC) mass concentrations are measured by a multi-angle absorption photometer (MAAP

hello 2018/4/24 9:09 PM

已删除: Finally,

hello 2018/4/24 9:09 PM

已删除: in section 4.4

hello 2018/4/24 9:11 PM

已删除: These three campaigns

hello 2018/4/8 6:24 PM

已删除: the AERONET BEIJING_PKU
station in Beijing (PKU),

hello 2018/4/8 6:15 PM

已删除: Of

hello 2018/4/9 7:07 PM

已删除: (Huairou)

hello 2018/4/8 6:25 PM

已删除: and t

China 2018/3/16 2:03 PM

已删除: are selected

175 model 5012, Thermo, Inc., Waltham, MA USA) at UCAS and by an Aethalometer 33 (Hansen et al.,
176 1984;Drinovec et al., 2015) at PKU and Gucheng. The aerosol σ_{sca} at wavelengths of 450 nm, 525 nm
177 and 635 nm is measured by an Aurora 3000 nephelometer and the corresponding values are recorded
178 every minute (Müller et al., 2011).

179 The f_{RH} is measured by a self-constructed humidified nephelometer system. The detail information
180 of the humidified nephelometer is described elsewhere (Kuang et al., 2017). Some brief descriptions
181 about the humidified nephelometer is introduced here. The humidifier is used to control the RH of the
182 sample aerosol and σ_{sca} is measured for each of the controlled RH. The sample aerosol is humidified
183 through a Gore-Tex tube, which is surrounded by a circulating water layer in a stainless steel tube. The
184 RH is changed by changing the temperature of the circulating water, which is controlled by the water
185 bath and software. For each cycle, the RH points are set to range from about 50% to about 90% over
186 45 minutes. For most of the cases, the aerosol PNSDs are consistent over the cycle. These cycles of f_{RH}
187 values are abandoned when the measured maximum and the minimum σ_{sca} value are beyond the range
188 of 1.4 and 0.6 times of the mean measured scattering coefficient of each cycle.

189 Ambient aerosol phase function at a time resolution of 5 minutes is measured at UCAS by using a
190 CCD-LADS. This system consists of a continuous laser, two charge-coupled device cameras and the
191 corresponding fish eye lenses. The wavelength of the laser is 532nm and a quarter-wave plate was
192 mounted in front of the laser emitter to change the polarization state of the laser from linear to circular.
193 The CCD-LADS can measure the ambient aerosol phase function at a wide angular range of 10-170°
194 with a high resolution of 0.1°. More details of the measurement system can be found at (Bian et al.,
195 2017).

196 3. Methodology

197 3.1 Calculating characteristics of g based on the Mie scattering theory (g_{Mie})

198 The Mie model (Bohren and Huffman, 2007) is employed to calculate the characteristics of g_{Mie} .
199 When running the Mie model, aerosol PNSD, aerosol complex refractive index, BC mixing state and
200 BC mass concentration are essential. Its results include aerosol phase function, and g_{Mie} can be
201 calculated by the definition shown in formula 2.

202 Mixing states of the BC come from the measurements of the field measurements. From the work
203 of Ma et al. (2012), the mixing states of BC in the NCP were presented as both core-shell mixed and

hello 2018/4/9 7:08 PM

已删除: Huairou

hello 2018/4/12 3:13 PM

已删除: (RH)

hello 2018/4/13 10:51 AM

已删除: with a time resolution of
approximately 45 min

hello 2018/4/9 7:08 PM

已删除: Huairou

hello 2018/4/12 3:11 PM

已删除: It

hello 2018/4/7 4:49 PM

已删除: g

hello 2018/4/13 12:32 PM

已删除: Its results include aerosol phase
function, and g can be calculated by the
definition shown in formula 2.

hello 2018/4/13 12:32 PM

已删除: necessary

hello 2018/4/13 1:00 PM

已删除: The complex refractive index of
non-absorbing aerosols is $1.53+10^{-7}i$ (Wex et
al., 2002b) at a wavelength of 525 nm. BC is
treated as partially internal mixed and the
remaining aerosols are treated as core-shell
mixed. The ratio of internally mixed BC mass
concentrations to core-shell mixed BC mass
concentration is determined by the method
introduced in

hello 2018/4/13 12:56 PM

已删除: Ma et al. (2012)

hello 2018/4/13 12:56 PM

已删除: . The size distribution of BC mass
concentration, which is adopted from

hello 2018/4/13 12:56 PM

已删除: Ma et al. (2012)

hello 2018/4/13 12:56 PM

已删除: is also used in this work. The
density and refractive index of BC are set as
 1.5 g/cm^3 and $1.8+0.54i$ (Kuang et al., 2015),
respectively. With this information, the value
of g under each measured PNSD at dry state
can be calculated.

externally mixed. Ma et al. (2012) provides the ratio of BC mass concentrations under an externally mixed state, M_{ext_BC} , to total BC mass concentration, M_{BC} , as follows:

$$r_{ext_BC} = \frac{M_{ext_BC}}{M_{BC}} \quad (5)$$

The mean value of $r_{ext_BC}=0.51$ (Ma et al., 2012) is used as a representation of the mixing state in this study. The size-resolved distribution of BC mass concentration is the same as that used by Ma et al. (2012). The κ -Köhler theory and the Mie scattering model are employed to calculate g_{Mie} under different RH conditions. When the aerosol gets hygroscopic growth, the BC is treated as non-hygroscopic and the water are assumed to mix only with the shell. The real time κ , which is derived from the measurement of f_{RH} , is used to account for aerosol hygroscopic growth. For each RH value, the growth factor can be calculated based on formula 3. The corresponding ambient aerosol PNSD at a given RH can be determined too by applying the κ and formula (4). The refractive index (\tilde{m}), which accounts for water content in the particle, is derived as a volume mixture between the dry aerosol and water (Wex et al., 2002a):

$$\tilde{m} = f_{v,dry} \tilde{m}_{aero,dry} + (1 - f_{v,dry}) \tilde{m}_{water} \quad (6)$$

where $f_{v,dry}$ is the ratio of the dry aerosol volume to the total aerosol volume under a given RH condition; $\tilde{m}_{aero,dry}$ is the refractive index for dry ambient aerosols and \tilde{m}_{water} is the refractive index of water.

The refractive indices of BC, non-light-absorbing aerosols and water, which are used in this study, are $1.8+0.54i$ (Kuang et al., 2015), $1.53+10^{-7}i$ (Wex et al., 2002b) and $1.33+10^{-7}i$, respectively. Then, the corresponding g values under the given RH and PNSD can also be calculated. More details on using the Mie model to calculate the aerosol phase function for different RH conditions can be found in Zhao et al. (2017).

3.2 Calculating g by using the random forest machine learning model (g_{ML})

In this study, the random forest machine learning model from the Scikit-Learn machine learning library (Hu et al., 2017; Pedregosa, 2011) was used to calculate . The random forest model has two parameters: the number of input variables (n_{pre}) and the number of trees grown (n_{tree}). In this study, the n_{pre} and n_{tree} are determined by minimize the relative difference of the g_{ML} and g_{Mie} . Details of choosing the values of n_{pre} and n_{tree} are shown in section 5 of the supplementary. The n_{pre} and n_{tree} are

hello 2018/4/13 12:52 PM
已设置格式: 居中

hello 2018/4/13 12:53 PM
已删除: .

hello 2018/4/20 9:17 AM
已删除: g

hello 2018/4/12 3:13 PM
已删除: (RH)

hello 2018/4/12 3:13 PM
已设置格式: 下标

hello 2018/4/7 4:52 PM
已删除: gf

hello 2018/4/13 1:36 PM
已设置格式: 字体:Symbol

hello 2018/4/24 9:51 PM
已删除: 4

hello 2018/4/13 12:57 PM
已删除: ,

hello 2018/4/13 1:21 PM
已设置格式: 缩进: 首行缩进: 0.74 cm

hello 2018/4/13 1:00 PM
已删除: is

hello 2018/4/16 1:48 PM
已删除: . The random forest model consists of a set of decision trees, and then, a simple majority vote from the decision tree is used for prediction. This model is a widely used nonparametric machine learning algorithm that has several strengths. First, it involves fewer assumptions regarding the dependence between observations and outcomes when compared with traditional parametric regression models. Second, strict relationships among variables are not needed before implementing the random forest model. .

hello 2018/4/24 9:24 PM

已删除: n_{pre} and n_{tree} are set as eight and ten, respectively.

284 set as eight and thirty two in this study, respectively. The eight input parameters include the three dry
285 scattering coefficients, three dry backscattering coefficients, RH and κ .

286 The measured datasets are divided into two parts: one for the training data of the random forest
287 model, and the other for test data. All training datasets come from field measurements at Gucheng
288 station, whereas the datasets from PKU are employed to test the accuracy of the model. With split
289 datasets from different sites, the feasibility of the random forest model in the NCP can be guaranteed.
290 Before calculating g_{Mie} , we compare the measured σ_{sca} from the dry nephelometer and calculate σ_{sca}
291 from the Mie scattering model. These data, where the relative difference between the measured and
292 calculated σ_{sca} is within 30%, are used for the following analyses. With this, the inaccuracy from the
293 measurement of the instruments can be avoided to some extent. More details regarding the used data
294 are shown in section 3 of the supplementary material.

295 To avoid the uncertainties of the measurements when training the random forest machine learning
296 model, both the required input parameters and the predictor g_{Mie} values, come from the calculation of
297 the Mie scattering model using the measurement of the aerosol PNSD and BC from the field campaign
298 of Gucheng. For each measured PSND and BC, the corresponding σ_{sca} and β_{sca} under dry condition at
299 the wavelength of 450nm, 525nm and 635nm are modeled based on the Mie theory. With the
300 concurrently measured κ values from the humidified nephelometer, the g values under different RH
301 can be determined too. Then the modeled σ_{sca} , β_{sca} under dry condition, the κ values and the RH are
302 used as the input data for the model and the corresponding g_{Mie} values are used as the predict data.

303 3.3 Aerosol DARF estimations

304 The earth-atmosphere systems can be significantly influenced by aerosols, which scatter and
305 absorb the energy. In this study, the Santa Barbara DISORT (discrete ordinates radiative transfer)
306 Atmospheric Radiative Transfer (SBDART) model (Ricchiazzi et al., 1998) is employed to estimate
307 the DARF. The characteristics of DARF with the variations in g are studied.

308 The instantaneous DARF is calculated at the TOA for cloud-free conditions. DARF is defined as
309 the difference between radiative flux at the TOA under present aerosol conditions and aerosol-free
310 conditions:

$$311 \quad \text{DARF} = (f_a \downarrow - f_a \uparrow) - (f_m \downarrow - f_m \uparrow) \quad (7)$$

312 where $(f_a \downarrow - f_a \uparrow)$ is the downward radiative irradiance flux with given aerosol distributions and
313 $(f_m \downarrow - f_m \uparrow)$ is the radiative irradiance flux under aerosol free conditions. The DARF at 50km is

hello 2018/4/23 10:44 AM

已删除: For these parameters, the ambient RH value come from automatic weather station, and the rest of the data come from the humidified nephelometer system measurements. The predictor g values are calculated from Mie scattering results.

hello 2018/4/23 10:45 AM

已删除: AERONET BEIJING_PKU

hello 2018/4/23 10:45 AM

已删除: Gucheng

hello 2018/4/7 5:06 PM

已删除: g

hello 2018/4/23 11:25 AM

已删除: 1.2

hello 2018/5/11 8:47 AM

已删除: ing

hello 2018/4/23 11:19 AM

已设置格式: 字体:Symbol

hello 2018/4/23 11:20 AM

已设置格式: 字体:Symbol

hello 2018/4/24 9:51 PM

已删除: 5

326 calculated because almost all of the aerosols are located at the range of 0 and 50km in the
327 parameterization scheme of aerosol vertical distribution (Liu et al., 2009). The wavelengths in the
328 range from 0.25 to 4 μm are calculated for irradiance in this study.

329 Input data for the SBDART are listed below. Vertical profiles of the aerosol optical properties,
330 which include the aerosol extinction coefficient (σ_{ext}), aerosol single scattering albedo (SSA) and g
331 with a height resolution of 50 m, come from results of the Mie scattering, and the parameterized
332 aerosol vertical distributions. Methods for parameterization and calculation of the aerosol optical
333 profiles can be found in section 4 of supplementary material or relate to Kuang et al. (2016) and Zhao
334 et al. (2017). Atmospheric meteorological parameter profiles come from the results of the intensive
335 radiosonde observations at the Meteorological Bureau of Beijing (39°48' N, 116°28' E) at the local
336 time of 13:30 from July to September in 2008. Kuang et al. (2016) studied these measured profiles and
337 found that the vertical distributions of these parameters, which include profiles for water vapor,
338 pressure and temperature, can be used as a good representation of the meteorological parameter
339 profiles in the NCP during the summer. The corresponding measured mean results during field
340 measurement are used in this study and the details of these profiles are shown in section 4 of the
341 supplementary material. Surface albedo values are obtained from the Moderate Resolution Imaging
342 Spectroradiometer (MODIS) V005 Climate Modeling Grid (CMG) Albedo Product (MCD43C3). The
343 mean results of the surface albedo of Beijing from Jul to September in 2008 are used. The remaining
344 input data for the SBDART are set to their default values (Ricchiuzzi et al., 1998).

345 4 Results and Discussion

346 4.1 Characteristics of g_{Mie}

347 4.1.1 Characteristics of g_{Mie} at different sites

348 Fig. 1 gives the statistical results for the calculated g properties at Gucheng, PKU and UCAS. The
349 RH at the three sites shows almost the same diurnal variation pattern in Fig. 1 (a) (b) and (c). The RH
350 reaches a peak in the morning at approximately 6:00 am, and then reaches its lowest value at
351 approximately 16:00 in the afternoon. However, the mean values of RH are 77.7%±20.9% at Gucheng,
352 47.8%±20.8% at PKU and 33.49±15.22% at UCAS. The g_{Mie} values under dry conditions that are
353 calculated by the measured PNSD have almost no diurnal patterns. The g_{Mie} values at PKU
354 (0.614±0.025) are slightly lower than those at Gucheng (0.601±0.021) and UCAS (0.595±0.023) as
355 shown in Fig. 1 (d), (e) and (f). The difference in g_{Mie} values results from different aerosol properties

hello 2018/4/16 8:17 PM

已删除: and t...he wavelengths for irradiance

hello 2018/4/13 8:19 PM

已删除: ation of...aerosol vertical

hello 2018/4/7 5:08 PM

已删除: g

hello 2018/4/7 5:08 PM

已删除: g

hello 2018/4/25 12:57 PM

已删除: and ... PKU and UCAS. The RH at

hello 2018/4/7 5:11 PM

已删除: g... values under dry conditions that

hello 2018/4/7 5:12 PM

已删除: g... values at PKU

hello 2018/4/7 5:12 PM

已删除: g

392 at these sites. From fig. S6, the peak diameter of the mean and median PNSD at Gucheng locates
393 around 150nm. However, the peak diameter of the mean and median PNSD at PKU locates at around
394 100nm. The peak values of the mean and median diameter of the aerosol PNSD at UCAS locates at
395 around 60nm. At the same time, there are large partitions of small particles that are lower than 60nm at
396 PKU and UCAS. However, these particles, which are lower than 100nm, contribute little to the total
397 aerosol scattering. The aerosol PNSD at PKU is more dispersed than that of the Gucheng and UCAS,
398 which corresponds to a larger variation in the g values. From fig. S6 (h), (i) and (j), the size
399 distribution of the aerosol scatter coefficient at around 500nm contributes less to the scatter coefficient
400 at PKU than at that of the Gucheng and UCAS. Thus these particles with the diameter larger than
401 500nm contribute more to the aerosol scattering coefficient. As g_{Mie} increase with the aerosol
402 diameter, the aerosol g_{Mie} under dry conditions at PKU tends to be larger than that at Gucheng and
403 UCAS.

404 However, ambient g_{Mie} values have different patterns at different sites, as shown in Fig. 1 (h), (i)
405 and (j). The g_{Mie} values have an RH-related diurnal pattern at Gucheng, with a mean value of
406 0.668 ± 0.073 , but show no diurnal variation at PKU and UCAS, where the mean values of g_{Mie} are
407 0.639 ± 0.049 and 0.618 ± 0.033 , respectively. The variations of ambient g_{Mie} values are mainly resulted
408 from the variation of the aerosol hygroscopic growth under the ambient condition, which is highly
409 related to the ambient RH. The g_{Mie} value is significantly influenced by RH when the RH is higher
410 than 80%, which will be detailed in section 4.1.2. Ambient g_{Mie} values at Gucheng, PKU and
411 UCAS can vary from 0.57 to 0.8, 0.55 to 0.76 and 0.56 to 0.72 respectively, comparable to those of
412 Andrews et al. (2006), which range from 0.59 to 0.72.

413 4.1.2 Influence of RH on g

414 To assess the influence of RH on g , the g_{Mie} values are calculated under different RH conditions
415 for each aerosol PNSD. The statistical results of g_{Mie} versus RH are shown in Fig. 2. The g_{Mie} value
416 has a mean of 0.61 at dry conditions and can vary widely (0.54 to 0.67), which corresponds to
417 approximately 10% of the variation. However, the mean g_{Mie} value can vary from 0.65 to 0.8 when
418 the RH reaches 90%. The g_{Mie} enhancement factor, which is defined as the ratio of g_{Mie} at a given
419 RH and g_{Mie} under dry conditions, can reach a mean value of 1.2 at an RH of 90%, which means that
420 the g_{Mie} value under wet conditions is approximately 20% higher than that under the dry conditions.

hello 2018/4/26 9:00 AM

已删除: two

hello 2018/5/11 8:54 AM

已删除: PKU

hello 2018/4/7 5:12 PM

已删除: g

hello 2018/4/26 9:12 AM

已删除: e

hello 2018/4/26 9:12 AM

已设置格式: 缩进: 左 0.56 字符, 首行缩进: 1.25 字符

hello 2018/4/26 9:13 AM

已删除: f

hello 2018/4/7 5:12 PM

已删除: g

hello 2018/4/20 9:18 AM

已删除: g

hello 2018/4/26 9:16 AM

已删除: is

hello 2018/4/26 9:13 AM

已删除: 15

hello 2018/4/26 9:14 AM

已删除: 028

hello 2018/4/7 5:13 PM

已删除: g

hello 2018/4/7 5:13 PM

已删除: g

hello 2018/4/7 5:14 PM

已删除: g

hello 2018/4/7 5:14 PM

已删除: g

hello 2018/4/7 5:14 PM

已删除: g

hello 2018/4/7 5:14 PM

已删除: g

hello 2018/4/7 5:14 PM

已删除: g

hello 2018/4/7 5:14 PM

已删除: g

hello 2018/4/7 5:15 PM

已删除: g

hello 2018/4/7 5:15 PM

已删除: g

441 This finding is consistent with that of Hartley and Hobbs (2001), who found that g is highly related to
442 the RH.

443 However, the aerosol complex refractive index has little influence on g and the uncertainties for g
444 are less than 0.004 based on the Monte Carlo simulation of the g at different complex refractive index.
445 More details of discussing the influence of aerosol complex refractive index on g can relate to section
446 6 of the supplementary materials.

447 4.2 Calculating g_{ML} by using the machine learning model

448 4.2.1 Feasibility of using the random forest model

449 We establish two independent random forest machine learning models to predict g_{ML} values
450 under dry conditions and under ambient RH conditions separately.

451 When running the random forest machine learning model for g values under dry conditions, σ_{sca}
452 and β_{sca} at three different wavelengths are used as the input for independent variables. The other two
453 input parameters, RH and κ , are set equal to zero. The predictor g values come from the results of the
454 Mie scattering model. Fig. 3(a) shows the calculated g_{Mie} values and predicted g_{ML} values by the
455 random forest machine learning model under dry conditions at the site of PKU. The results show that
456 the g_{Mie} values and g_{ML} values show good consistency with an R^2 value of 0.98. There are 95% of
457 the cases that the relative difference between g_{Mie} and g_{ML} are within the relative differences of 2.56%.

458 Fig. 3(b) shows the comparison of the predicted g_{ML} values under different RH condition and
459 g_{Mie} values calculated by the Mie scattering model. The correlation coefficient between g_{Mie} and g_{ML}
460 reaches 0.93 and 95% of the relative differences within 4.02%. The random forest model can be a good
461 method to predict g values under different RH conditions with high accuracy and the uncertainties of
462 predicting g values using the random forest machine learning model is estimated to be 4.02%.

463 The filled colors of the dots in Fig. 3 represent the concurrently measured σ_{sca} . It is shown that
464 with an increase in σ_{sca} , g values tend to be larger, which is in accordance with the particle scattering
465 properties. When a particle has larger diameters, the σ_{sca} of the particle is higher, and there tends to be
466 a larger partition of forward scattering light.

467 Wiscombe and Grams (1976) studied the relationship between b and g and gave the expression
468 between them as follows:

469
$$g = -7.143889 \cdot b^3 + 7.464439 \cdot b^2 - 3.96356 \cdot b + 0.9893 \quad (8).$$

hello 2018/4/24 9:57 PM

已设置格式: 缩进: 首行缩进: 0.74 cm

hello 2018/4/7 5:15 PM

已删除: g

hello 2018/4/7 5:17 PM

已删除: g

hello 2018/4/24 9:48 PM

已删除: , measured by an Aurora 3000
nephelometer, ...re used as the input for [6]

hello 2018/4/7 5:18 PM

已删除: g...values and the random forest [7]

hello 2018/4/7 5:18 PM

已删除: g...values by the random forest [8]

hello 2018/4/20 9:19 AM

已删除: predicted g values

hello 2018/4/20 9:19 AM

已设置格式: 字体:加粗

hello 2018/4/20 9:19 AM

已设置格式: 字体:非 加粗

hello 2018/4/24 9:22 AM

已删除: 0... The corresponding deviations in [9]

hello 2018/4/24 9:27 AM

已删除: To predict ambient g values, the RH
is set at ambient values, and κ is set to
concurrently derived values from the
humidified nephelometer system. ... [10]

hello 2018/4/7 5:21 PM

已删除: g

hello 2018/4/7 5:21 PM

已删除: g...values calculated by the Mie [11]

hello 2018/4/24 9:51 PM

已删除: 6

512 This equation is widely used to calculate g from b (Andrews et al., 2006; Horvath et al.,
 513 2016; Kassianov et al., 2007). We use the field measurement results to test its reliability. The
 514 comparison results between calculated g values from the Mie scattering model and parameterized g
 515 values from equation 6 are shown in Fig.S3. From Fig.S3, we can see that the parameterized g values
 516 are prevalently larger than the calculated g values by approximately 10%. When the σ_{sca} is smaller, the
 517 deviations become larger. Some other empirical relationships between b and g (Moosmüller and
 518 Ogren, 2017) are also tested. These parameterization scheme has almost the same result as Wiscombe
 519 and Grams (1976). This result means that the previously established parameterization scheme is not
 520 applicable in the NCP

521 4.2.2 Sensitivity of the random forest model

522 Sensitivity studies are carried out to assess the influence of each input variable on g_{ML} . Based on
 523 the works of Müller et al. (2011), the uncertainties in total scattering are 4% (450nm), 2% (525nm), 5%
 524 (635nm) for experiments with ambient air and laboratory generated white particles. For backscattering,
 525 the differences are higher and amount 7% (450nm), 3% (525nm) and 11% (635nm). The uncertainties
 526 of the measured RH by the RH sensors is 1.7% for RH ranges from 0 to 90% (Kuang et al., 2017) and
 527 the uncertainties of the derived κ values is 6% (Kuang et al., 2017). The Monte Carlo simulations are
 528 conducted to study the sensitivities of the g_{ML} to the input parameters in three steps. First, the mean
 529 results of the measured dry σ_{sca} , dry β_{sca} , RH and κ values are used to predict the g value. Second, the
 530 dry σ_{sca} at 450 nm are randomly changed with a mean value of 0 and standard deviation of 4% and the
 531 other input are kept unchanged as the input. The corresponding standard deviation of the predicted g
 532 value is used as the sensitivities of the predicted g values to the σ_{sca} at 450nm. At last, the sensitivities
 533 are carried out accordingly for each of the input parameter. With this, the uncertainties of the g_{ML}
 534 values to the input parameters are estimated. The total uncertainties of predicting g RH are derived
 535 when all of the input parameters are randomly changed with their corresponding uncertainties. For
 536 each test, the Monte Carlo simulations are carried out for 20000 times.

537 Table 2 gives the two time of the standard deviation of the g_{ML} values corresponding to the
 538 uncertainties of the input parameters. Form table 2, it is shown that the uncertainties of measured σ_{sca}
 539 has little influence of the g_{ML} with 0.487%, 0.492% and 0.486% for wavelength of 450nm, 525nm and
 540 635nm respectively. However, the measurement of the three β_{sca} have larger uncertainties and lead to
 541 greater influence on predicting g_{ML} with 0.651%, 0.486% and 0.710%. The uncertainty of the RH has

China 2018/3/16 2:21 PM

已删除: 5

hello 2018/4/24 9:38 AM

已删除: This result means that the previously established parameterization scheme is not applicable in the NCP

hello 2018/4/7 5:22 PM

已删除: g

hello 2018/4/20 8:04 PM

已删除: First, we run the random forest model with measured input variables and record predicted g values. These g values are marked as g_0 . Second, input test variables are randomly increased or decreased by 5% percent of the measured values and are used as new input variables. Then, the input variables are used to predict g values, which are compared with g_0 . Finally, each variable is changed by 10% and 20% separately, and deviations of the predicted g are studied.

hello 2018/4/23 1:28 PM

已设置格式: 两端对齐

hello 2018/4/20 8:20 PM

已设置格式: 字体: Symbol

558 little influence on predicting g_{ML} with 0.487%. However, the uncertainty of derived κ values (6%)
559 influence the g values most with 1.92%. The total uncertainties of predicting g due to the uncertainties
560 of the measurement is 1.95%. All in all, the total uncertainties of predicting the g_{ML} is estimated to be
561 4.47% considering the 4.02% uncertainties of the random forest machine learning model from section
562 4.2.1.

564 4.2.3 Validation of the random forest machine learning model

565 Datasets of the UCAS campaign are also used to validate the random forest machine learning
566 model. On one hand, the g_{ML} values are calculated by using the random forest machine learning
567 model with the measurements of the humidified nephelometer. On the other hand, ambient g values are
568 calculated by using the measured phase function from the CCD-LADS g_{CCD} according to the
569 definition shown in formula 2. Then the g values calculated with the two methods are compared.

570 Comparison results of these two kinds of g values are shown in fig. 4. From fig. 4, the values of
571 g_{ML} and g_{CCD} show good consistence. There are 95% of the conditions that the relative differences
572 between the g_{ML} and g_{CCD} are in the range of 6.5% which is a little higher than the relative
573 difference of the g values (4.02%) between machine learning method and the Mie scattering method.
574 During the period, the σ_{sca} range from 30 to 260 Mm^{-1} which lead to cleaner conditions in UCAS than
575 in Gucheng and PKU. Correspondingly, most of the g_{Mie} values are small and locate at the range of
576 0.54 to 0.62 which are obviously lower than those in other campaigns. At the same time, the
577 surrounding condition at UCAS during the winter is relative dry, which results to small g values. These
578 conditions may partially explain the relatively higher difference between the g_{ML} and g_{CCD} . With this
579 validation, we conclude that the random forest machine learning model can give a reasonable g value
580 based on the measurements of the humidified nephelometer system.

581 4.3 Estimating the impacts of g on DARF

582 4.3.1 Uncertainties of replacing the calculated phase function with the PF_{HG}

583 When the PF_{HG} is used to parameterize the calculated phase function by using the Mie theory
584 (PF_{Mie}), there are some deviations and the influence of these deviations should be estimated. The
585 relative difference between the DARF from the (PF_{Mie}) and from the PF_{HG} is used to estimate
586 uncertainties when using the PF_{HG} . First, the PF_{Mie} profiles are used as inputs to estimate DARFs. The
587 PF_{Mie} is then replaced with the g -related PF_{HG} which is parameterized by g_{Mie} from the PF_{Mie} , and the

hello 2018/4/24 9:20 AM

已删除: Fig. 4 gives the results of the deviations of g due to variations in each variable. The results show that when the input test variables change by 5%, the predicted g values are mainly sensitive to the given κ with a variation of 1.74%. A 5% variation in RH can lead to a 1.17% variation in predicted g . However, g is not sensitive to the single measured σ_{sca} and β_{sca} variables. This finding

hello 2018/4/24 10:27 AM

已删除: 7

hello 2018/4/24 10:28 AM

已删除: 7

hello 2018/4/24 1:53 PM

已删除: 90

hello 2018/4/24 10:47 AM

已删除: 6

hello 2018/4/7 12:49 PM

已删除: real

hello 2018/4/24 12:58 PM

已删除: HG phase function

hello 2018/4/24 12:58 PM

已删除: HG phase function

hello 2018/4/7 12:49 PM

已删除: actual

hello 2018/4/7 12:50 PM

已删除: actual

hello 2018/4/7 12:50 PM

已删除: phase function

hello 2018/4/24 1:00 PM

已删除: the DARF

hello 2018/4/24 12:58 PM

已删除: HG phase function

hello 2018/4/24 12:58 PM

已删除: HG phase function

hello 2018/4/7 12:50 PM

已删除: actual

hello 2018/4/24 1:00 PM

已删除: calculated aerosol phase function

hello 2018/4/24 1:00 PM

已删除: phase function

hello 2018/4/24 12:58 PM

已删除: HG phase function

DARFs are calculated again. These relative differences between the DARFs from the above two steps are recorded and compared. The relative differences at different zenith angle conditions are calculated to comprehensively estimate the influence of the HG phase function.

Fig.5 shows the estimated DARFs at different zenith angles. In Fig. 5(a), DARF at the TOA can vary from -2.55 to -4.8 w/m^2 . When the PF_{Mie} is replaced by the PF_{HG} , the calculated DARF ranges from -2.6 to -5.1 w/m^2 . The relative difference of the DARFs between the two methods ranges from 1.3% to 7.1%, as shown in Fig. 5(b). It is concluded that using the g-related PF_{HG} to replace the PF_{Mie} to estimate aerosol radiative effects is applicable, with a deviation of less than 7%, in the NCP.

4.3.2 Impacts of g variations on DARF estimation

Variations in g can lead to significant variations in the estimated DARF (Kuang et al., 2016; Andrews et al., 2006; McComiskey et al., 2008). In this study, the uncertainties of the g values from the input parameter is estimated to be 1.95% when predicting g and the total variation in running the random forest machine learning model is estimated to be 4.47%. At the same time, the g can vary about 10% for different aerosol PNSD and can be enhanced by 20% with the increment of RH from 30% to 90%. It is very important to know the extent of the variation in DARF corresponding to the uncertainties from g.

The variation in DARF from the uncertainties of g is calculated by increasing or decreasing g by 1.95%, 4.47%, and 10% to the original g values, and then comparing the corresponding DARFs with the original DARFs. To study the influence of RH on g and DARF, the DARF with the g values calculated from the dry parameterized aerosol population profile, is estimated.

Fig. 6 shows the estimated DARFs with different variation in g and the corresponding variation in the estimated DARF. The results show that when g varies by 1.95%, the DARF can vary 4%. However, variations of 4.47% and 10% in g values can lead to variations in the estimated DARF with 9.4% and 21%, respectively. The estimated DARF using the parameterized aerosol profile, which considers the aerosol hygroscopic growth, is smaller than the DARF using the g profiles from the dry aerosol population. The g values under dry condition are smaller than that of the wet ambient. Thus, there is larger partition of energy that is scattered forward which leads to less outgoing backscattering energy and a larger value of the estimated DARF. When the DARF are estimated ignoring the impacts of aerosol hygroscopic growth on g, the relative difference can be as high as 20% for all of the zenith angles. It is necessary to considering the aerosol hygroscopic growth when calculating the g values.

hello 2018/4/24 1:01 PM

已删除: phase function...is replaced by the

hello 2018/4/24 8:04 PM

已删除: We study the influence of g on
DARF...he variation in DARF from the

hello 2018/4/24 8:05 PM

已删除: ...fig. 6 shows the estimated DARF

5 Conclusions

The characteristics of g in the NCP are studied based on the Mie scattering theory and field measurements from sites of Gucheng and PKU. The results show that g_{Mie} values are 0.604 ± 0.025 at Gucheng and 0.615 ± 0.021 at PKU. The ambient g_{Mie} values at Gucheng show obvious diurnal variations due to variations in RH. When the ambient RH reaches 90%, g_{Mie} can be enhanced by 20% and the g values under different aerosol population can vary 10%. Comparison of the calculated g_{Mie} values from the Mie scattering model and the parameterized g values from the Wiscombe and Grams (1976) method shows that the parameterized g is overestimated by approximately 10% and that the deviations are even greater when the measured σ_{sca} is below 200 Mm^{-1} .

The random forest machine learning model and datasets from the humidified nephelometer are employed to calculate g_{ML} values. The input data of the random forest model contain measured σ_{sca} and β_{sca} at three wavelengths, RH and the hygroscopic parameter κ . Except for RH, all input data came from measurements from the humidified nephelometer system (Kuang et al., 2017). The random forest model can significantly improve the accuracy of predicting g_{ML} . The uncertainties of the predicted g_{ML} values are constrained to be within 2.56% under dry conditions and 4.02% under ambient conditions and the uncertainties from the measurement of the humidified nephelometer can lead to a variation of 1.95% in g , which is mainly resulted from the inaccuracy of the derived κ . The total uncertainty of calculating g using the random forest machine learning model is 4.47%. This is the first time that datasets from the humidified nephelometer system and machine learning are combined to study g . At the same time, this method can accounting for the influence of aerosol hygroscopic growth on g .

The new method for calculating g is validated by comparing the g_{ML} values from the random forest machine learning model and the g_{CCD} values from the measured phase function by using the CCD-LADS. The g values with this two methods show good consistence with 95% of the data within the relative difference of 6.5%.

SBDART model is used to study the impacts of g on DARF. We first studied the relative differences between the estimated DARFs by using the PF_{HG} and the calculated phase function by using the Mie theory, the measured mean aerosol PNSD and BC mass concentration at the site of PKU. The results show that the relative differences in DARF can be contained within 7.1% when replacing

hello 2018/4/24 8:36 PM

已删除: At the same time, the influences of ignoring the variations in g with RH are studied by estimating the DARF with g profiles varying with the RH and the DARF with g profiles of the dry condition. ... [16]

hello 2018/4/7 5:29 PM

已删除: g

hello 2018/4/7 5:29 PM

已删除: g

hello 2018/4/7 5:29 PM

已删除: g ... can be enhanced by 20% and ... [17]

hello 2018/4/7 5:30 PM

已删除: g

hello 2018/4/7 5:30 PM

已删除: g ... values. The input data of the ... [18]

hello 2018/4/7 5:30 PM

已删除: g ... Tand t ... [19]

hello 2018/4/7 5:30 PM

已删除: g ... values are constrained to be ... [20]

hello 2018/4/24 3:05 PM

已设置格式: 字体: Symbol

hello 2018/4/24 3:01 PM

已删除: A sensitivity study of the random forest model shows that the predicted g is sensitive to ambient RH and the aerosol hygroscopic parameter κ .

hello 2018/4/7 5:31 PM

已删除: g ... values calculated by using ... [21]

hello 2018/4/7 5:31 PM

已删除: g ... values calculated ... from the ... [22]

hello 2018/4/24 8:44 PM

已删除: HG phase function... F_{HG} and ... [23]

775 the PF_{Mie} with g -related PF_{HG} . The HG phase function can be a feasible parameterization scheme to
776 study DARF in the NCP.

777 The sensitivity study shows that the maximum uncertainties of DARF are 4%, 9.4% and 21%,
778 which correspond to the uncertainties of the g from the instrument measurement, the machine learning
779 model and the variation of aerosol PNSD. However, when the DARF are estimated ignoring the effects
780 of aerosol hygroscopic growth on g , the relative differences of the DARF is as large as 20% for all of
781 the zenith angles. It is necessary to parameter the g with accounting for the effect of aerosol
782 hygroscopic growth.

783 This work can further our understanding of the role of g in the radiative effects of aerosols and can
784 help reduce uncertainties in estimating DARF.

786 **Acknowledgements**

787 This work is supported by the National Natural Science Foundation of China (41590872) and the
788 National Key R&D Program of China (2016YFC020000:Task 5).

790 **References**

791 Andrews, E., Sheridan, P. J., Fiebig, M., McComiskey, A., Ogren, J. A., Arnott, P., Covert, D., Elleman, R., Gasparini, R.,
792 Collins, D., Jonsson, H., Schmid, B., and Wang, J.: Comparison of methods for deriving aerosol asymmetry parameter,
793 Journal of Geophysical Research, 111, 10.1029/2004jd005734, 2006.

794 Bian, Y., Zhao, C., Xu, W., Zhao, G., Tao, J., and Kuang, Y.: Development and validation of a CCD-laser aerosol detective
795 system for measuring the ambient aerosol phase function, Atmos. Meas. Tech., 10, 2313-2322,
796 10.5194/amt-10-2313-2017, 2017.

797 Bian, Y. X., Zhao, C. S., Ma, N., Chen, J., and Xu, W. Y.: A study of aerosol liquid water content based on hygroscopicity
798 measurements at high relative humidity in the North China Plain, Atmospheric Chemistry and Physics, 14, 6417-6426,
799 10.5194/acp-14-6417-2014, 2014.

800 Bohren, C. F., and Huffman, D. R.: Absorption and Scattering by a Sphere, in: Absorption and Scattering of Light by Small
801 Particles, Wiley-VCH Verlag GmbH, 82-129, 2007.

802 Boucher, O.: On Aerosol Direct Shortwave Forcing and the Henyey–Greenstein Phase Function, J Atmos Sci, 55, 128-134,
803 10.1175/1520-0469(1998)055<0128:OADSFA>2.0.CO;2, 1998.

804 Breiman, L.: Random Forests, Machine Learning, 45, 5-32, 10.1023/a:1010933404324, 2001.

805 Charlson, R. J., Porch, W. M., Waggoner, A. P., and Ahlquist, N. C.: Background aerosol light scattering characteristics:
806 nephelometric observations at Mauna Loa Observatory compared with results at other remote locations, Tellus, 26,
807 345-360, 1974.

808 D'Almeida, G. A., Koepke, P., and Shettle, E. P.: Atmospheric Aerosols: Global Climatology and Radiative Characteristics,
809 Journal of Medical Microbiology, 54, 55-61, 1991.

810 Drinovec, L., Močnik, G., Zotter, P., Prévôt, A. S. H., Ruckstuhl, C., Coz, E., Rupakheti, M., Sciare, J., Müller, T.,

hello 2018/4/24 1:20 PM

已删除: actual calculated phase function

hello 2018/4/7 12:55 PM

已删除:

hello 2018/4/24 1:20 PM

已删除: HG phase function

hello 2018/4/24 8:45 PM

已删除:

hello 2018/4/24 8:45 PM

已设置格式: 缩进: 首行缩进: 0.74 cm

hello 2018/4/24 8:50 PM

已删除: variations of 10% and 20% from g can lead to variations in DARF of 20% and 39%, respectively.

hello 2018/4/24 8:50 PM

已删除: T

Wiedensohler, A., and Hansen, A. D. A.: The "dual-spot" Aethalometer: an improved measurement of aerosol black carbon with real-time loading compensation, *Atmospheric Measurement Techniques*, 8, 1965-1979, 10.5194/amt-8-1965-2015, 2015.

Formenti, P., Andreae, M. O., and Lelieveld, J.: Measurements of aerosol optical depth above 3570 m asl in the North Atlantic free troposphere: results from ACE - 2, *Tellus B*, 52, 678-693, 10.1034/j.1600-0889.2000.00006.x, 2000.

Hansen, A. D. A., Rosen, H., and Novakov, T.: The aethalometer — An instrument for the real-time measurement of optical absorption by aerosol particles, *Science of The Total Environment*, 36, 191-196, [http://dx.doi.org/10.1016/0048-9697\(84\)90265-1](http://dx.doi.org/10.1016/0048-9697(84)90265-1), 1984.

Hansen, J. E.: EXACT AND APPROXIMATE SOLUTIONS FOR MULTIPLE SCATTERING BY CLOUDY AND HAZY PLANETARY ATMOSPHERES, *J Atmos Sci*, 26, 478-&, 10.1175/1520-0469(1969)026<0478:eaasfm>2.0.co;2, 1969.

Hartley, W. S., and Hobbs, P. V.: An aerosol model and aerosol-induced changes in the clear-sky albedo off the east coast of the United States, *Journal of Geophysical Research: Atmospheres*, 106, 9733-9748, 10.1029/2001jd900025, 2001.

Horvath, H., Kasahara, M., Tohno, S., Olmo, F. J., Lyamani, H., Alados-Arboledas, L., Quirantes, A., and Cachorro, V.: Relationship between fraction of backscattered light and asymmetry parameter, *Journal of Aerosol Science*, 91, 43-53, 10.1016/j.jaerosci.2015.09.003, 2016.

Hu, X., Belle, J. H., Meng, X., Wildani, A., Waller, L. A., Strickland, M. J., and Liu, Y.: Estimating PM2.5 Concentrations in the Conterminous United States Using the Random Forest Approach, *Environ Sci Technol*, 51, 6936-6944, 10.1021/acs.est.7b01210, 2017.

Huttunen, J., Kokkola, H., Mielonen, T., Mononen, M. E. J., Lipponen, A., Reunanen, J., Lindfors, A. V., Mikkonen, S., Lehtinen, K. E. J., Kouremeti, N., Bais, A., Niska, H., and Arola, A.: Retrieval of aerosol optical depth from surface solar radiation measurements using machine learning algorithms, non-linear regression and a radiative transfer-based look-up table, *Atmospheric Chemistry and Physics*, 16, 8181-8191, 10.5194/acp-16-8181-2016, 2016.

Kassianov, E. I., Flynn, C. J., Ackerman, T. P., and Barnard, J. C.: Aerosol single-scattering albedo and asymmetry parameter from MFRSR observations during the ARM Aerosol IOP 2003, *Atmos. Chem. Phys.*, 7, 3341-3351, 10.5194/acp-7-3341-2007, 2007.

Kuang, Y., Zhao, C. S., Tao, J. C., and Ma, N.: Diurnal variations of aerosol optical properties in the North China Plain and their influences on the estimates of direct aerosol radiative effect, *Atmos. Chem. Phys.*, 15, 5761-5772, 10.5194/acp-15-5761-2015, 2015.

Kuang, Y., Zhao, C. S., Tao, J. C., Bian, Y. X., and Ma, N.: Impact of aerosol hygroscopic growth on the direct aerosol radiative effect in summer on North China Plain, *Atmospheric Environment*, 147, 224-233, 2016.

Kuang, Y., Zhao, C., Tao, J., Bian, Y., Ma, N., and Zhao, G.: A novel method for deriving the aerosol hygroscopicity parameter based only on measurements from a humidified nephelometer system, *Atmos. Chem. Phys.*, 17, 6651-6662, 10.5194/acp-17-6651-2017, 2017.

Kudo, R., Nishizawa, T., and Aoyagi, T.: Vertical profiles of aerosol optical properties and the solar heating rate estimated by combining sky radiometer and lidar measurements, *Atmospheric Measurement Techniques*, 9, 3223-3243, 10.5194/amt-9-3223-2016, 2016.

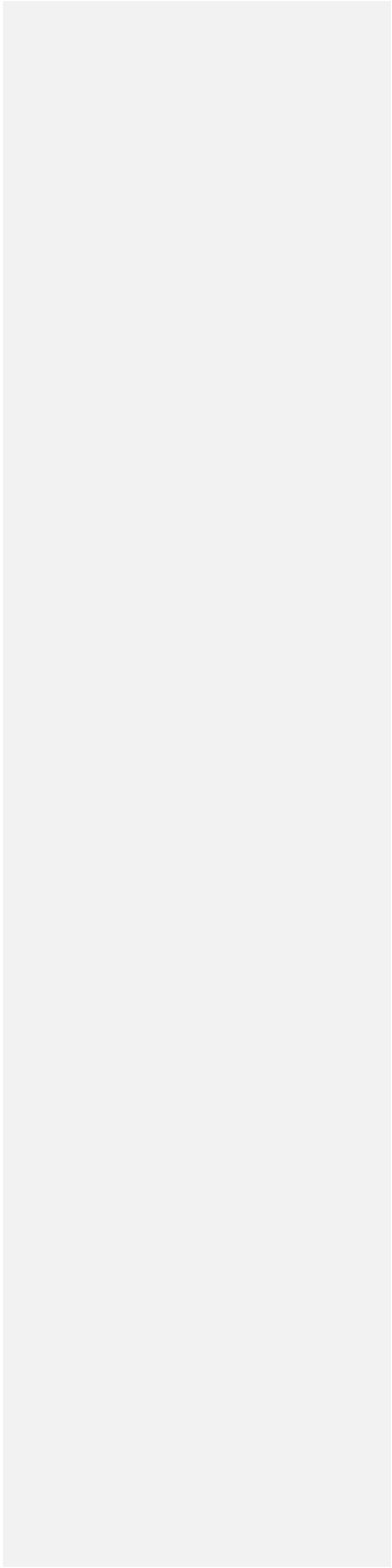
Liu, P., Zhao, C., Zhang, Q., Deng, Z., Huang, M., Xincheng, M. A., and Tie, X.: Aircraft study of aerosol vertical distributions over Beijing and their optical properties, *Tellus Series B-Chemical & Physical Meteorology*, 61, 756-767, 2009.

Ma, N., Zhao, C. S., Müller, T., Cheng, Y. F., Liu, P. F., Deng, Z. Z., Xu, W. Y., Ran, L., Nekat, B., van Pinxteren, D., Gnauk, T., Müller, K., Herrmann, H., Yan, P., Zhou, X. J., and Wiedensohler, A.: A new method to determine the mixing state of light absorbing carbonaceous using the measured aerosol optical properties and number size distributions, *Atmos. Chem. Phys.*, 12, 2381-2397, 10.5194/acp-12-2381-2012, 2012.

Ma, N., Zhao, C., Tao, J., Wu, Z., Kecorius, S., Wang, Z., Größ, J., Liu, H., Bian, Y., Kuang, Y., Teich, M., Spindler, G., Müller, K., van Pinxteren, D., Herrmann, H., Hu, M., and Wiedensohler, A.: Variation of CCN activity during new particle formation

863 events in the North China Plain, *Atmospheric Chemistry and Physics*, 16, 8593-8607, 10.5194/acp-16-8593-2016, 2016.
 864 Marshall, S. F., Covert, D. S., and Charlson, R. J.: Relationship between asymmetry parameter and hemispheric backscatter
 865 ratio: implications for climate forcing by aerosols, *Applied Optics*, 34, 6306-6311, 10.1364/AO.34.006306, 1995.
 866 McComiskey, A., Schwartz, S. E., Schmid, B., Guan, H., Lewis, E. R., Ricchiazzi, P., and Ogren, J. A.: Direct aerosol forcing:
 867 Calculation from observables and sensitivities to inputs, *Journal of Geophysical Research Atmospheres*, 113, -, 2008.
 868 Moosmüller, H., and Ogren, J. A.: Parameterization of the Aerosol Upscatter Fraction as Function of the Backscatter
 869 Fraction and Their Relationships to the Asymmetry Parameter for Radiative Transfer Calculations, *Atmosphere*, 8, 133,
 870 10.3390/atmos8080133, 2017.
 871 Müller, T., Laborde, M., Kassell, G., and Wiedensohler, A.: Design and performance of a three-wavelength LED-based total
 872 scatter and backscatter integrating nephelometer, *Atmos. Meas. Tech.*, 4, 1291-1303, 10.5194/amt-4-1291-2011, 2011.
 873 Pandey, A., and Chakrabarty, R. K.: Scattering directionality parameters of fractal black carbon aerosols and comparison
 874 with the Henyey-Greenstein approximation, *Opt Lett*, 41, 3351-3354, 10.1364/OL.41.003351, 2016.
 875 Pedregosa, F., Varoquaux, G., Gramfort, A., Michel, V., Thirion, B., Grisel, O., Blondel, M., Prettenhofer, P., Weiss, R.,
 876 Dubourg, V., Vanderplas, J., Passos, A., Cournapeau, D., Brucher, M., Perrot, M., and Duchesnay, E.: Scikit-learn: Machine
 877 Learning in Python, *J. Mach. Learn. Res.*, 12, 2825-2830, 2011.
 878 Petters, M. D., and Kreidenweis, S. M.: A single parameter representation of hygroscopic growth and cloud condensation
 879 nucleus activity, *Atmos. Chem. Phys.*, 7, 1961-1971, 10.5194/acp-7-1961-2007, 2007.
 880 Ricchiazzi, P., Yang, S., Gautier, C., and Sowle, D.: SBDART: A Research and Teaching Software Tool for Plane-Parallel
 881 Radiative Transfer in the Earth's Atmosphere, *Bulletin of the American Meteorological Society*, 79, 2101-2114,
 882 10.1175/1520-0477(1998)079<2101:sarats>2.0.co;2, 1998.
 883 Ross, J. L., Hobbs, P. V., and Holben, B.: Radiative characteristics of regional hazes dominated by smoke from biomass
 884 burning in Brazil: Closure tests and direct radiative forcing, *Journal of Geophysical Research Atmospheres*, 103, 31925–
 885 31941, 1998.
 886 Russell, P. B., Kinne, S. A., and Bergstrom, R. W.: Aerosol climate effects: Local radiative forcing and column closure
 887 experiments, *Journal of Geophysical Research Atmospheres*, 102, 9397-9407, 1997.
 888 Sagan, C., and Pollack, J. B.: Anisotropic nonconservative scattering and the clouds of Venus, *Journal of Geophysical*
 889 *Research*, 72, 469-477, doi:10.1029/JZ072i002p00469, 1967.
 890 Shettle, E. P., and Fenn, R. W.: Models for the aerosols of the lower atmosphere and the effects of humidity variations on
 891 their optical properties, *Lancet*, 48, 504, 1979.
 892 Tao, J. C., Zhao, C. S., Ma, N., and Liu, P. F.: The impact of aerosol hygroscopic growth on the single-scattering albedo and
 893 its application on the NO₂ photolysis rate coefficient, *Atmos. Chem. Phys.*, 14, 12055-12067, 10.5194/acp-14-12055-2014,
 894 2014.
 895 Toublanc, D.: Henyey-Greenstein and Mie phase functions in Monte Carlo radiative transfer computations, *Applied Optics*,
 896 35, 3270-3274, 10.1364/ao.35.003270, 1996.
 897 Wex, H., Neususs, C., Wendisch, M., Stratmann, F., Koziar, C., Keil, A., Wiedensohler, A., and Ebert, M.: Particle scattering,
 898 backscattering, and absorption coefficients: An in situ closure and sensitivity study, *J Geophys Res-Atmos*, 107,
 899 10.1029/2000jd000234, 2002a.
 900 Wex, H., Neusüß, C., Wendisch, M., Stratmann, F., Koziar, C., Keil, A., Wiedensohler, A., and Ebert, M.: Particle scattering,
 901 backscattering, and absorption coefficients: An in situ closure and sensitivity study, *Journal of Geophysical Research:*
 902 *Atmospheres*, 107, LAC 4-1-LAC 4-18, 10.1029/2000jd000234, 2002b.
 903 Wiscombe, W. J., and Grams, G. W.: The Backscattered Fraction in two-stream Approximations, *J Atmos Sci*, 33,
 904 2440-2451, 10.1175/1520-0469(1976)033<2440, 1976.
 905 Zhao, G., Zhao, C., Kuang, Y., Tao, J., Tan, W., Bian, Y., Li, J., and Li, C.: Impact of aerosol hygroscopic growth on retrieving
 906 aerosol extinction coefficient profiles from elastic-backscatter lidar signals, *Atmos. Chem. Phys. Discuss.*, 2017, 1-24,

907 10.5194/acp-2017-240, 2017.
908
909
910



911

912 **Table 1.** Field information, dataset information and instruments that are used in this study.

Field information		Datasets and instruments				
Location	Time period	PSND	BC	σ_{sc}	f_{RH}	Phase function
Gucheng, Hebei (39°09' N, 115°44' E)	15 Oct to 25 Nov, 2016	SMP, APS	AE33	Aurora 3000	Humidified Nephelometer	None
PKU, Beijing (39°59' N, 116°18' E)	21 Mar to 10 Apr, 2017	SMPS, APS	AE33	Aurora 3000	Humidified Nephelometer	None
UCAS, Beijing (40°24' N, 116°40' E)	3 Jan to 27 Jan, 2016	SMPS, APS	MAAP	Aurora 3000	Humidified Nephelometer	CCD- LADS

hello 2018/4/12 3:14 PM

已删除: (RH)

hello 2018/4/12 3:14 PM

已设置格式: 下标

hello 2018/4/9 7:08 PM

已删除: Huairou

913

914

917 **Table 2.** The sensitivities of g to the input parameters.

Parameter	$\sigma_{\text{sca},450}$	$\sigma_{\text{sca},525}$	$\sigma_{\text{sca},635}$	$\beta_{\text{sca},450}$	$\beta_{\text{sca},525}$	$\beta_{\text{sca},635}$	RH	κ	total
Parameter(%) ^{*1}	4	2	5	7	3	11	6	6	
g(%) ^{*2}	0.487	0.492	0.486	0.651	0.487	0.710	0.486	1.920	1.950

918 *1. The uncertainties of the measured parameters.

919 *2. The uncertainties of g values due to the uncertainties of the measurement parameters.

920

hello 2018/4/23 3:01 PM

已设置格式: 字体:Symbol

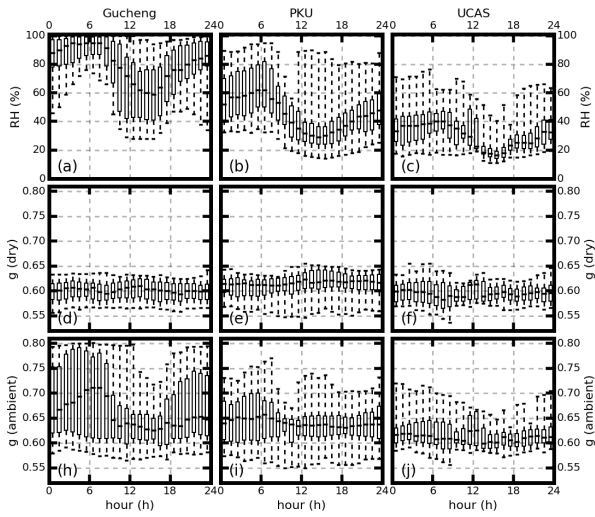
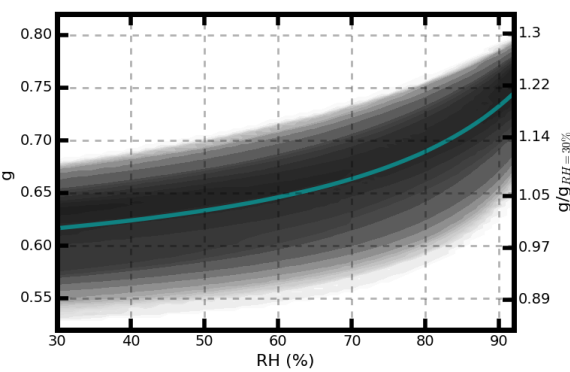
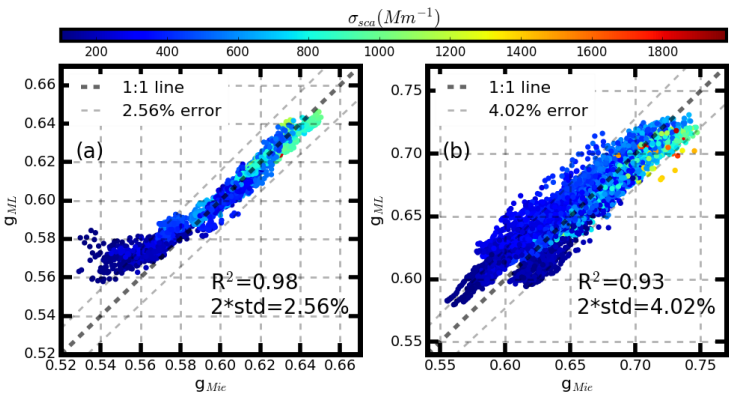


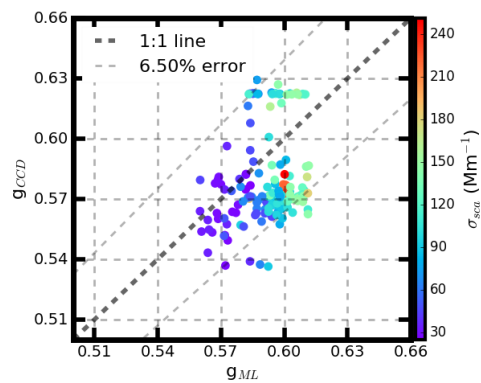
Figure 1. (a)(b)(c) Average diurnal pattern of RH, (d)(e)(f) g values calculated from dry aerosols, and (h)(i)(g) g values from ambient aerosols. The panels (a), (d) and (h) are the results from Gucheng. Panels (b), (e) and (i) are the results from PKU. Panels (c),(f) and (g) are the results of UCAS. The box and whisker plots represent the 5th, 25th, 75th and 95th percentiles.



928 **Figure 2.** Probability distributions of g under different RH conditions. The ticks on the left show g
929 values at different RH values, and the ticks on the right show the g enhancement factor, which is
930 defined as the ratio of g at a given RH to the g value at dry conditions (RH=30%). The solid line (cyan)
931 shows the mean result of g values and the enhancement factor at different RH values.
932

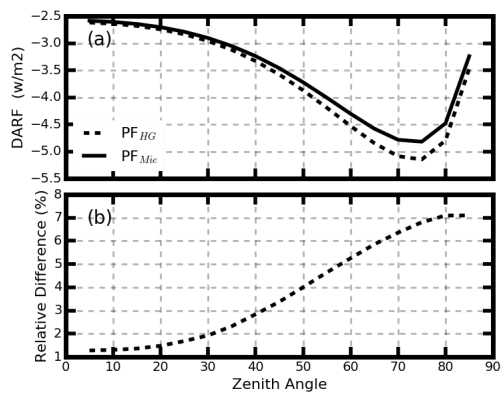


935 **Figure 3.** Comparison of calculated g values (g_{Mie}) from the Mie model and predicted g values (g_{ML})
936 | from the random forest model under (a) dry conditions and (b) ambient conditions [at the site of PKU](#).
937 Colored dots represent the concurrently measured σ_{sca} corresponding to the time of g .



938 **Figure 4.** Comparison of the calculated g values (g_{CCD}) from the CCD-LADS measured phase function
 939 and the calculated g values (g_{ML}) by using the random forest machine learning model.

hello 2018/4/24 12:43 PM
 已删除: the calculated g values ($g_{\text{Machine,cal}}$)
 by using the random forest machine learning
 model and
 hello 2018/4/24 12:43 PM
 已删除: .cal
 hello 2018/4/24 12:43 PM
 已删除: .



948

949

950

951

952

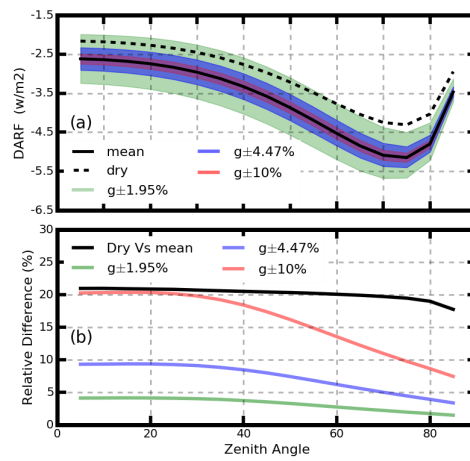
Figure 5. (a) Estimated DARFs at different zenith angles when using the g -related HG phase function (dotted line) and the phase function calculated by using the Mie scattering theory (solid line). (b) The relative difference between the DARFs in (a).

hello 2018/4/7 12:55 PM

已删除:

hello 2018/4/24 1:48 PM

已删除: calculated



956 | **Figure 6.** The variation in DART when g varies by a range of 1.95% (the filled dark color), 10% (grey
 957 color), and 20% (light grey color). Different line styles represent the corresponding mean relative
 958 differences in DART compared to the original value.

hello 2018/4/24 7:49 PM

已删除: 2.3